2008

Rad54B targeting to DNA double-strand break repair sites requires complex formation with S100A11

Ulrike Murzik
Friedrich Schiller Universitat, Jena

Peter Hemmerich
Leibniz Institute for Age Research

Stefanie Weidtkamp-Peters
Leibniz Institute for Age Research

Tobias Ulbricht
Leibniz Institute for Age Research

Wendy Bussen
Washington University School of Medicine in St. Louis

See next page for additional authors

Molecular Biology of the Cell
Vol. 19, 2926–2935, July 2008

Rad54B Targeting to DNA Double-Strand Break Repair Sites Requires Complex Formation with S100A11

Ulrike Murzik,* Peter Hemmerich,† Stefanie Weidtkamp-Peters,†‡ Tobias Ulbricht,† Wendy Bussen,§‖ Julia Hentschel,* Ferdinand von Eggeling,* and Christian Melle*

*Core Unit Chip Application (CUCA), Institute of Human Genetics and Anthropology, Medical Faculty, Friedrich-Schiller-University, 07740 Jena, Germany; †Department of Molecular Biology, Fritz Lipmann Institut (FLI), Leibniz Institute for Age Research, 07708 Jena, Germany; and §Department of Molecular Biophysics and Biochemistry, Yale University School of Medicine, New Haven, CT 06515

Submitted November 20, 2007; Revised March 14, 2008; Accepted April 24, 2008
Monitoring Editor: M. Bishr Omary

S100A11 is involved in a variety of intracellular activities such as growth regulation and differentiation. To gain more insight into the physiological role of endogenously expressed S100A11, we used a proteomic approach to detect and identify interacting proteins in vivo. Hereby, we were able to detect a specific interaction between S100A11 and Rad54B, which could be confirmed under in vivo conditions. Rad54B, a DNA-dependent ATPase, is described to be involved in recombinational repair of DNA damage, including DNA double-strand breaks (DSBs). Treatment with bleomycin, which induces DSBs, revealed an increase in the degree of colocalization between S100A11 and Rad54B. Furthermore, S100A11/Rad54B foci are spatially associated with sites of DNA DSB repair. Furthermore, while the expression of $p21^{WAF1/CIP1}$ was increased in parallel with DNA damage, its protein level was drastically down-regulated in damaged cells after S100A11 knockdown. Down-regulation of S100A11 by RNA interference also abolished Rad54B targeting to DSBs. Additionally, S100A11 down-regulated HaCaT cells showed a restricted proliferation capacity and an increase of the apoptotic cell fraction. These observations suggest that S100A11 targets Rad54B to sites of DNA DSB repair sites and identify a novel function for S100A11 in p21-based regulation of cell cycle.

INTRODUCTION

Proteins may exist in several complexes in a spatial and temporal manner to accomplish distinct functions. Analyses of the interacting partners will provide a strong insight into the physiological role of a particular factor. Therefore, it is essential to identify ideally all interacting partners of proteins in vivo to precisely be able to define their biological function. The investigation of protein complexes of solely endogenously expressed proteins avoid the tendency to detect false positive protein–protein interactions of examinations performed in vitro. A multitude of proteins are involved in both the detection and the repair of DNA damages. It is conceivable that some protein complexes involved in these processes are not yet discovered. A severe form of DNA damage that threaten the integrity of the genome are DNA double-strand breaks (DSBs). DSBs can lead to cell cycle arrest or illegitimate DNA rearrangements that can contribute to cell dysfunction, cell death, or carcinogenesis (Hoeijmakers, 2001). Homologous recombination is a major DNA repair pathway by which DSBs are repaired (Lettier *et al.*, 2006).

For the identification of specific interacting proteins of S100A11 (S100C, calgizzarin) we used in the present study a proteomic approach comprising mass spectrometry and immunological techniques. S100A11 belongs to the group of S100 proteins that are considered as multitasking proteins involved in several biological processes such as the Ca^{2+} signaling network, cell growth and motility, cell cycle progression, transcription, and cell differentiation (Schafer and Heizmann, 1996; Donato, 2001; Eckert *et al.*, 2004). It has been proposed that the S100 proteins are involved in the differentiation of specific tissues including epidermis and that some members of this family are differentially expressed in normal human skin and melanocytic lesions (Boni *et al.*, 1997). In several studies, S100A11 was detected to be up- and down-regulated in different tumors including melanoma (van Ginkel *et al.*, 1998; Chaurand *et al.*, 2001; Melle *et al.*, 2006). S100A11 plays a dual role in growth regulation in human keratinocytes as it is able to mediate a Ca^{2+}-induced growth inhibition as well as it stimulates the growth by enhancement of the level of EGF family proteins (Sakaguchi *et al.*, 2003, 2008). During growth inhibition, S100A11 is specifically phosphorylated by PKCα that is a prerequisite for binding to nucleolin and transfer into the nucleus. In the nucleus, a functional cascade activates the cell cycle modulatory properties of $p21^{WAF1/CIP1}$ (Sakaguchi *et al.*, 2004). The activity of p21 is typically induced by p53 and results in an arrest of the cell cycle in G1 through the

This article was published online ahead of print in *MBC in Press* (http://www.molbiolcell.org/cgi/doi/10.1091/mbc.E07–11–1167) on May 7, 2008.

Present addresses: ‡ Lehrstuhl für Molekulare Physikalische Chemie, Institut für Physikalische Chemie, Heinrich-Heine-Universität Düsseldorf, 40225 Düsseldorf, Germany; ‖ Department of Radiation Oncology, Washington University School of Medicine, St. Louis, MO 63108.

Address correspondence to: Christian Melle (christian.melle@mti.uni-jena.de).

inhibition of CDKs (El-Deiry *et al.*, 1993; Dulic *et al.*, 1994). This allows repair of possible DNA damages before the next replication cycle. In cells containing only a mutated form of p53, alternative induction pathways of the p21 activity occurs, and its expression can be positively regulated through several p53-independent mechanisms (Gartel and Tyner, 1999; Tsuda *et al.*, 2005; Fang *et al.*, 2007). One of these induction mechanisms of p21 seems to be mediated by S100A11 (Sakaguchi *et al.*, 2003). The aim of this study was to identify endogenously expressed interacting partners of S100A11 and to investigate their functional interplay in human cells.

MATERIALS AND METHODS

Cell Culture

The human keratinocyte cell line HaCaT (Boukamp *et al.*, 1988) was cultured in DMEM supplemented with 10% fetal bovine serum.

For protein–protein interaction experiments cells were grown to 80% confluence and were passaged at a split ratio of 1:4. Cells were harvested at 70–90% confluence and lysed in a buffer containing 100 mM sodium phosphate, pH 7.5, 5 mM EDTA, 2 mM $MgCl_2$, 0.1% CHAPS, 500 μM leupeptin, and 0.1 mM PMSF. After centrifugation (15 min; 15,000 rpm) the supernatant was immediately used.

Antibodies

Anti-S100A11 rabbit polyclonal antibody (BC001410; Protein Tech Group, Chicago, IL), anti-Rad54B rabbit polyclonal antibody (Wesoly *et al.*, 2006), anti-Rad54 mouse mAb (ab11055; Abcam, Cambridge, MA), anti-actin rabbit polyclonal antibody (A266; Sigma, St. Louis, MO), and normal rabbit IgG (PeproTech, Rocky Hill, NJ) were used in protein–protein interaction detection assays as well as in coimmunoprecipitation experiments. Anti-S100A11 chicken polyclonal antibody (ab15612; Abcam), anti-Rad54B rabbit polyclonal antibody (Wesoly *et al.*, 2006), anti-SC-35 mouse mAb (S4045; Sigma), anti-Rad54 mouse mAb (ab11055; Abcam), anti-Ku80 mouse mAb (AB-4/N3H10; Labvision, Fremont, CA), anti-PCNA (proliferating cell nuclear antigen) mouse mAb (PC 10; Santa Cruz Biotechnology, Santa Cruz, CA), and anti-γH2AX (Ser139; clone JBW301; Upstate Biotechnology, Lake Placid, NY) were used in two- or three-color immunofluorescence staining as primary antibodies, which were detected with species-specific secondary antibodies linked to fluorescein, Cy3 or Cy5 (Dianova, Rodeo, CA).

Protein–Protein Complex Detection Assay

The protein–protein complex detection assay was described elsewhere (Escher *et al.*, 2007). Briefly, 20 μl of Interaction Discovery Mapping (IDM) beads (Bio-Rad, Richmond, CA) were incubated with 4 μl protein A (Sigma) overnight at 4°C. A pellet was generated by centrifugation, and the supernatant was discarded. The pellet was washed twice with a buffer containing 50 mM sodium acetate, pH 5.0. Afterward, the beads were incubated in a buffer containing 0.5 M Tris/HCl, pH 9.0, 0.1% Triton X-100 for 2 h at room temperature for blocking residual reactive groups. The beads were washed three times with 1× PBS. Thereafter, a specific antibody against human S100A11 or normal rabbit IgG as negative control, in 50 mM sodium acetate, pH 5.0, was applied to the beads and allowed to bind at room temperature for 1 h at 4°C in an end-over-end mixer. Unbound antibody was removed by washing in 50 mM sodium acetate. Afterward, the beads were washed in 1× PBS, 0.1% Triton X-100 and in 1× PBS and incubated with 250 μl of crude HaCaT cell extract for 2 h at 4°C in an end-over-end mixer. The unbound proteins were washed away by sequential washes in PBS, 0.5 M sodium chloride, 0.05% Triton X-100 in PBS, PBS, and aqua bidest. Bound proteins were eluated from the IDM beads by 25 μl 50% acetonitrile/0.5% trifluoroacetic acid and gently vortexed for 30 min. Five microliters of the eluated samples were applied to the activated, hydrophobic surface of an H50 ProteinChip Array (Bio-Rad) and dried on air. After washing with 3 μl aqua bidest, 0.5 μl sinapinic acid (saturated solution in 0.5% TFA/50% acetonitrile) was applied twice and the array was analyzed in a ProteinChip Reader (series 4000; Bio-Rad) according to an automated data collection protocol by SELDI-MS. This includes an average of 265 laser shots to each spot with a laser intensity of 2300 and 3500 nJ, respectively, dependent on the measured region (low = 2.5–20 kDa and high = 20–200 kDa, respectively) and an automatically adapted detector sensitivity.

Peptide Fingerprint Mapping

Peptide fingerprint mapping was carried out as described elsewhere (Escher *et al.*, 2007). In brief, the volume of eluated samples was reduced to a maximum of 10 μl using a speed-vac (ThermoSavant, Fisher Scientific, Pittsburgh, PA) and subjected to SDS-PAGE for separation of containing proteins followed by staining with Simply Blue Safe Stain (Enhanced Coomassie, Invitrogen, Carlsbad, CA). Specific gel bands were excised, destained, and dried, followed by rehydration and digestion with 10 μl of a trypsin solution (0.02 μg/μl; Promega, Madison, WI) at 37°C overnight. The supernatants of the in-gel digestions were applied directly to NP20 arrays (Bio-Rad). After addition of the matrix (CHCA), peptide fragment masses were analyzed using the ProteinChip Reader, series 4000 instrument. A standard protein mix (all-in-1 peptide standard mix; Bio-Rad), including Arg8-vasopressin (1082.2 Da), somatostatin (1637.9 Da), dynorphin (2147.5 Da), ACTH (2933.5 Da), and insulin beta-chain (3495.94 Da) was used for calibration. Proteins were identified using the fragment masses searching in a publicly available database (http://prowl.rockefeller.edu/prowl-cgi/profound.exe).

Coimmunoprecipitation

The coimmunoprecipitation (coIP) assays were carried out as described (Escher *et al.*, 2007). Briefly, specific anti-S100A11 or anti-Rad54B antibody, respectively, or, as negative control, normal rabbit IgG were bound on protein A-agarose beads. Crude extract (100 μl) from HaCaT cells was incubated with the antibody loaded beads for 1 h at 4°C. Then the resins were washed three times with coIP buffer containing 20 mM HEPES/KOH, pH 8.0, 50 mM KCl, 0.1 mM EDTA, and 0.05% CHAPS. Bound proteins were subjected to 10% SDS-PAGE and detected by immunoblotting.

Immunocytochemistry and Confocal Microscopy

Cells grown on coverslips were fixed by treatment with methanol at −20°C for 5 min followed by acetone (prechilled to −20°C) for 2 min or by incubation in 2% paraformaldehyde for 20 min at room temperature followed by acetone treatment (prechilled to −20°C) for 2 min. Immunofluorescence was performed as previously described (von Mikecz *et al.*, 2000). Samples were scanned with a Zeiss LSM 510 laser scanning confocal device attached to an Axioplan 2 microscope using a 63× Plan-Apochromat oil objective (Carl Zeiss, Jena, Germany). Fluorescein, Cy3, or Cy5 dyes were excited by laser light at a 488-, 552-, or 633-nm wavelength, respectively. To avoid bleed-through effects in double- or triple-staining experiments, each dye was scanned independently using the multitracking function of the LSM 510 U. Single optical sections were selected either by eye-scanning the sample in *z*-axis for optimal fluorescence signals or were taken from stack projections. Images were electronically merged using the LSM 510 (Carl Zeiss) software and stored as TIFF files. Figures were assembled from the TIFF files using Adobe Photoshop software (San Jose, CA).

Colocalization Analysis

Colocalization in image pairs was assessed from scatter plots of midnuclear confocal images as described previously (von Mikecz *et al.*, 2000) and quantified using the LSM 510 META software (Carl Zeiss). The colocalization coefficient for two signals was determined according to Manders *et al.* (1993), which provides a value range between 0 and 1 (0, no colocalization; 1, all pixels colocalize). Only signals above a threshold gray value of 100 (of four-bit images, gray value intensity 0–255) were considered for the colocalization analysis.

Induction of DNA Damages by Bleomycin

HaCaT cells were seeded at six-well plates on coverslips for 16 h. DMEM supplemented with 10% fetal calf serum (FCS) was exchanged to fresh DMEM supplemented with 10% FCS, and cells were treated with 12.5 IU/ml bleomycin (BLM). Medium was exchanged after 30 min, and cells were harvested after different time points.

Colony-forming Assay

To assess the survival rate of cells after BLM treatment, 10^4 cells were seeded into 10-cm Petri dishes. After 24 h, the cells were treated with different concentrations of the drug and cultured for another 10 d. In control treatments, single cells had formed colonies of ~30 cells after that time. Colonies were then washed once with PBS, fixed with methanol for 15 min, stained with Giemsa dye, and finally air-dried. The number of colonies formed was then determined.

Small Interfering RNA–mediated Knockdown of S100A11

Small interfering RNA (siRNA) duplex oligonucleotides used in this study are based on the human cDNAs encoding S100A11. S100A11 siRNA as well as a nonsilencing control siRNA were obtained from QIAGEN GmbH (Hilden, Germany). The siRNA sequences applied to target S100A11 were 5′-GAACUAGCUGCCUUCACAAdTdT-3′ (sense) and 5′-UUGUGAAGGCAGCUAGUUCdTdG-3′ (antisense). The siRNA sequences used as negative controls were 5′-UUCUCCGAACGUGUCACGUdTdT-3′ (sense) and 5′-ACGUGACACGUUCGGAGAAdTdT-3′ (antisense). HaCaT (2×10^5) were plated on six-well plates 18 h before transfection and were 50% confluent when siRNA was added. The amount of siRNA duplexes applied was 1.5 μg/well for S100A11. Transfection was performed using the amphiphilic delivery system SAINT-RED (Synvolux Therapeutics B.V., Groningen, The Nether-

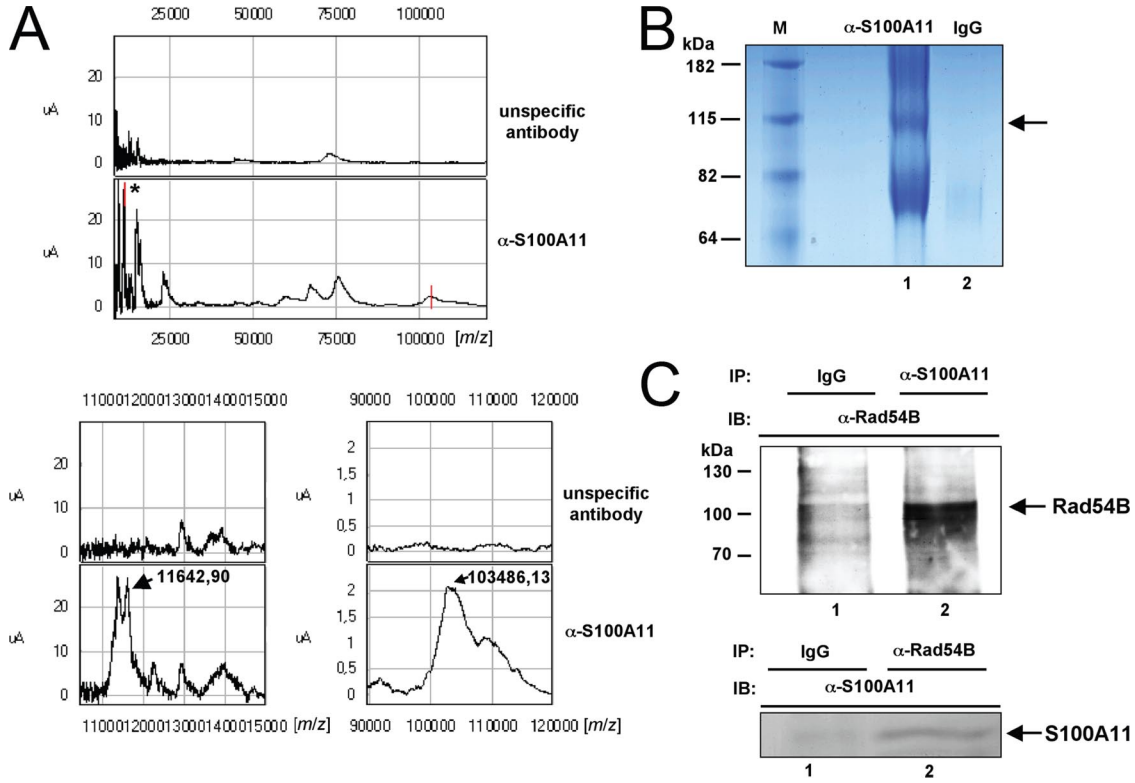

Figure 1. Detection and identification of the DNA-dependent ATPase Rad54B as a specific interacting protein of S100A11 by a protein–protein complex detection assay. (A) An anti-S100A11 antibody was coupled on IDM beads and incubated with HaCaT cell extract. Bound proteins were analyzed by SELDI-MS. Top, spectra of the measured area of m/z 0–120,000; bottom, the enlarged area of m/z 11,000–13,000 or m/z 90,000–120,000, respectively. A number of specific peaks were detectable in the assay using the S100A11 antibody compared with the experiments using an unspecific antibody. Among a signal of approx. 11.7 kDa, which corresponds well to the relative molecular mass of S100A11 (labeled by a peak tic and an asterisk in the top panel), a signal at approx. 103.5 kDa was detectable (labeled by peak tic only in the top panel) using the specific anti-S100A11 antibody. Both signals were absent in the assay using an unspecific antibody. (B) Eluted proteins from IDM beads were subsequently subjected on an SDS-PAGE for separation and a specific band at ~105 kDa (labeled by an arrow) was excised and used for a tryptic in-gel digestion. Peptide mass fingerprints obtain from digestion were analyzed by SELDI-MS and used for a database quest that revealed Rad54B. (C) For an unequivocally confirmation of this result, a coimmunoprecipitation was used. Thereby, a specific anti-S100A11 antibody was capable to precipitate Rad54B from HaCaT cell extract as shown in an immunoblot (lane 2). coIP using an unspecific antibody detected no signal (lane 1). In a reciprocal experiment an anti-Rad54B antibody precipitated S100A11 (lane 2, bottom panel) compared with the negative control (lane 1, bottom panel).

lands) according to the manufacturer's instructions. Briefly, siRNA was complexed with 15 nmol of transfection reagent and added to the cells for 4 h. Subsequently, 2 ml of culture medium was added and incubation proceeded for 72 h.

In colony-forming assays as well as in flow-cytometric experiments, HaCaT cells were retransfected with the specific S100A11 siRNA or a nonsilencing control siRNA after 72 h for a stable down-regulation of S100A11.

RESULTS

Identification of Rad54B as an Interacting Protein of S100A11

S100A11 appears to be involved in a number of cellular processes. Therefore, it is assumed that S100A11 interacts with a number of specific proteins to achieve several functions. It is conceivable that some of these interacting partners are not yet discovered. For this reason, we first performed a protein–protein complex detection assay to identify interacting proteins of endogenously expressed S100A11 in crude extracts of HaCaT cells, an immortalized human keratinocyte line (Boukamp *et al.*, 1988). This assay was used previously for the identification of protein complexes involved in cell cycle regulation as well as of the transcription machinery (Escher *et al.*, 2007; Kob *et al.*, 2007). S100A11-containing protein complexes were captured by a specific antibody against S100A11 coupled to IDM beads followed by elution of the captured proteins and analysis of the complex composition using SELDI-MS (Figure 1A). Hereby, a specific signal possessing an m/z of 11642 was detected that corresponds very well to the relative molecular mass of S100A11. Beside this signal and other specific peaks, we captured an additional specific signal of approx. 103 kDa. Signals derived from S100A11 and at 103 kDa were absent in the negative control using an unspecific antibody. For identification of the 103-kDa signal we subjected the eluted proteins to SDS-PAGE and detected a specific band in the range of approx. 105 kDa. Thus, we confirmed the presence of a specific S100A11-interacting protein. The negative control using rabbit IgG as unspecific antibody did not show a band at that position (Figure 1B). This specific band was excised from the gel and subsequently subjected to an in-gel digestion by trypsin and protein identification. As a control, an empty gel piece underwent the same treatment. The digest yielded solution was spotted on a NP20 array and the peptide mass fingerprints (PMF) were determined by SELDI-MS. Database searches (Profound; http://prowl.rockefeller.edu/prowl-cgi/profound.exe) revealed Rad54B as the best candi-

date with an estimated Z-score of 1.33. Rad54B is a homolog of the DNA repair and recombination protein RAD54 as well as a DNA-dependent ATPase and seems to play an unique role in homologous recombination (Miyagawa *et al.,* 2002; Tanaka *et al.,* 2002). Additionally and as an internal control for the detection of protein–protein interactions in vivo using our approach, we confirmed the well-known protein interaction between S100A11 and actin (Supplemental Figure S1; Xhao *et al.,* 2000). The protein complex between S100A11 and actin occurs temporally and spatially in a manner different from the complex containing S100A11 and Rad54B, because S100A11 interacts with actin exclusively in the cytoplasm.

To confirm the presence of protein complexes containing S100A11 and Rad54B, coIP experiments were carried out with crude extracts of HaCaT cells. In line with the previously determined results, a specific antibody that recognizes S100A11 was able to coprecipitate Rad54B (Figure 1C, top panel). In the negative control using an unspecific antibody, a clear signal corresponding to Rad54B was not detectable. Additionally, we were able to coprecipitate S100A11 by a specific anti-Rad54B antibody in a reciprocal coIP (Figure 1C, bottom panel). Hereby, we detected an, albeit slight, but clearly detectable signal compared with the negative control using the unspecific antibody. A reason for this only slightly coprecipitated signal corresponding to S100A11 might be that solely endogenous proteins were investigated. These results suggest that endogenous S100A11 and endogenous Rad54B exist, at least transiently, in one and the same stable protein complex.

S100A11 and Rad54B Colocalize in the Nucleus of Human Cells

Afterward, we examined the subcellular localization of S100A11 and Rad54B by immunofluorescence experiments on HaCaT cells followed by confocal laser scanning microscopy. S100A11 is described to localize predominantly in the nucleus of gliomablastoma cells and in both, the cytoplasm and the nucleus of normal human epidermis cells (Inada *et al.,* 1999; Broome *et al.,* 2003). Rad54B was described to contribute to homologous recombination-mediated DNA damage repair (Wesoly *et al.,* 2006). On the basis of this function, Rad54B is expected to predominantly localize to the nucleus. Both S100A11 as well as Rad54B were found concentrated at discrete sites throughout the nucleoplasm of human HaCaT cells (Figure 2). The colocalization analysis revealed significant, albeit not complete, overlap between S100A11 and Rad54B in this foci-like pattern. These observations are consistent with the finding that S100A11 and Rad54B reside within the same complexes endogenously (Figure 1) and suggest that these complexes are enriched in a dot-like pattern within the nucleoplasm. No or very little colocalization could be detected between S100A11 or Rad54B, respectively, and the non-snRNP (small nuclear ribonucleoproteins) splicing factor SC-35, which concentrates in a speckle like pattern (Supplemental Figure S2; Bisotto *et al.,* 1995). This result indicates that the regions of overlap between S100A11 and Rad54B are not coincidental (see also Figure 3B). In contrast to these results, a protein–protein interaction or colocalization, respectively, between S100A11 and Rad54 was neither detectable in coIP experiments nor in immunofluorescence experiments (Supplemental Figure S3).

Complex Formation between S100A11 and Rad54B Is Stimulated by DNA Damage

It is supposed that Rad54B plays an unique role in homologous recombination (Miyagawa *et al.,* 2002). Homologous recombination is one of the major repair pathways when DSBs occur as a consequence of application of DNA-damaging agents (Wolner *et al.,* 2003). We therefore determined whether BLM, a DNA-damaging agent, would influence the dynamics of the colocalization between S100A11 and Rad54B in HaCaT cells. First, we determined BLM treatment conditions that induced the formation of DSBs but would not kill the cells (Supplemental Figure 4). H2AX becomes phosphorylated as one of the first cellular responses after DNA damage and forms foci at sites of DSBs (Rogakou *et al.,* 1998). Incubation of U2OS cells with 12.5 IU/ml for 30 min was sufficient to produce 30–40 γH2AX foci 3 h after drug application. After 24 h the number of γH2AX foci dropped to control levels, indicating successful repair of most, if not all, DNA DSBs. A colony-forming assay of cells treated with increasing amounts of BLM confirmed that cells treated with 12.5 IU/ml BLM are viable, proliferate, and had therefore successfully repaired their DSBs. Similar results were obtained with both U2OS and HaCaT cells.

Qualitatively, the induction of DNA DSBs in HaCaT cells by BLM treatment caused an obvious increase of colocalization between S100A11 and Rad54B during the repair process, as indicated by an increase in yellow signals over time (Figure 3A). This up-regulation was accompanied by an increase of coprecipitated Rad54B/S100A11 complexes (Figure 3B). The degree of colocalization in the nucleus was therefore quantitated during the complete repair cycle (Figure 3C). A significant increase in colocalization between nuclear S100A11 and Rad54B foci was already observed 30 min after BLM application. Colocalization persisted at that high level for 3 h, after which it decreased again to pretreatment levels (Figure 3C). Interestingly, the kinetics of colocalization between S100A11 and Rad54B perfectly mirrored the kinetics of the DNA DSB repair based on γH2AX foci formation (compare Figure 3C and Supplemental Figure S4). The colocalization of S100A11 and Rad54B at sites of DNA DSB repair appears to be specific and not coincidental because the degree of colocalization between either S100A11 or Rad54B with foci containing the functionally unrelated splicing factor SC-35 (speckles) was significantly smaller after BLM treatment (Figure 3C).

To assess if this protein complex is specifically linked to DNA damage sites, we next carried out three-color confocal immunostaining to simultaneously detect S100A11, Rad54B,

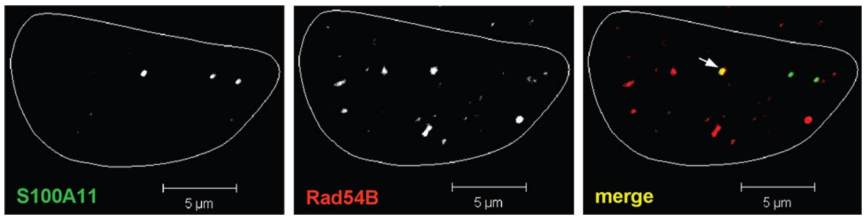

Figure 2. Colocalization of S100A11 and Rad54B in the nucleoplasmic foci. Fixed HaCaT cells were coimmunostained with anti-S100A11 (green) and anti-Rad54B antibody (red). The merged image reveals significant colocalization between S100A11 and Rad54B in a dot-like pattern throughout the nucleoplasm of HaCaT cells. A colocalized S100A11/Rad54B complex is labeled by an arrow.

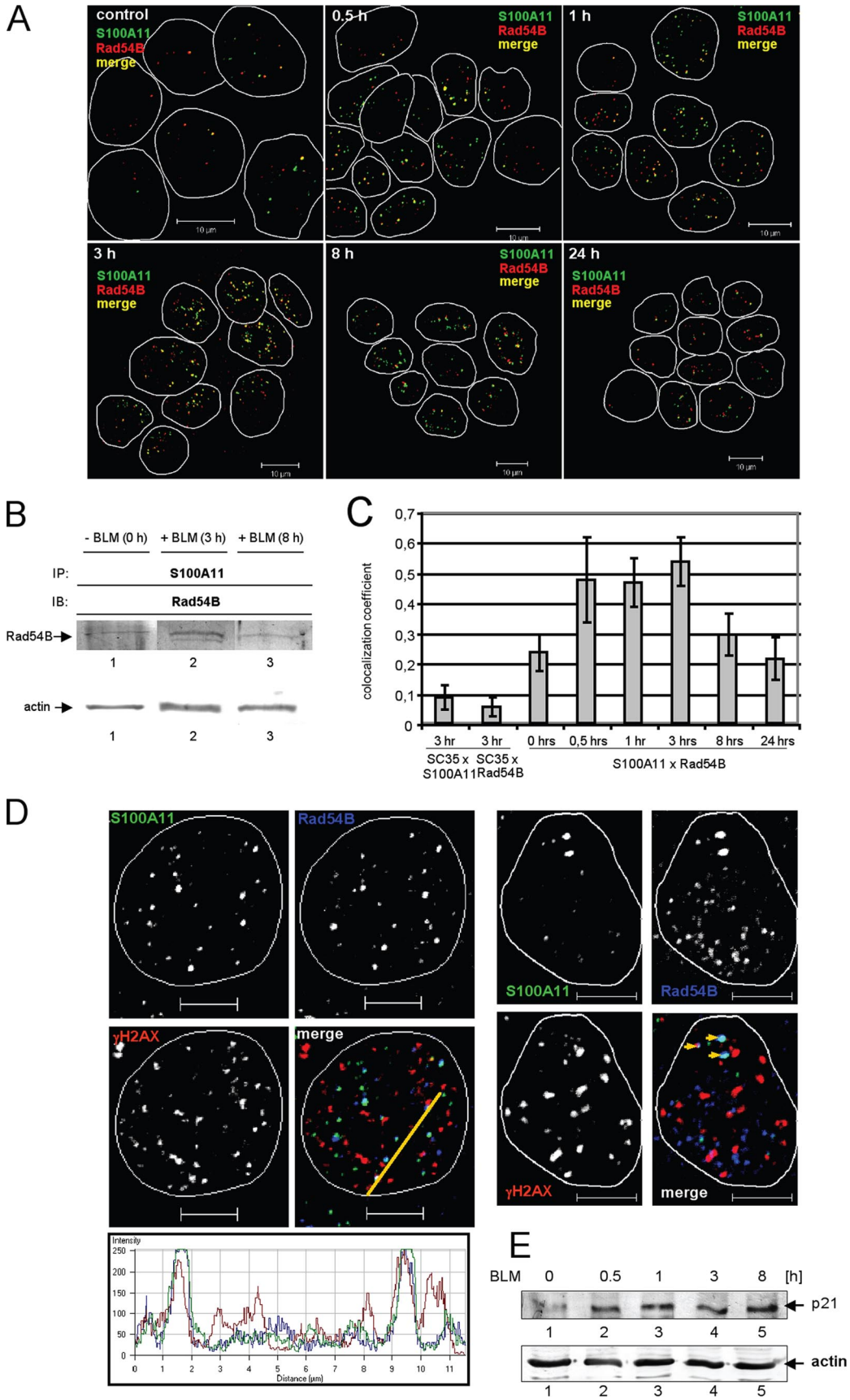

Figure 3. DNA DSBs induce an increase in S100A11/Rad54B foci formation. (A) HaCaT cells were treated with bleomycin (BLM; 12.5 μg ml^{-1}) and analyzed by two-color immunostaining followed by laser scanning microscopy for S100A11 (green) and for Rad54B (red) or

and γH2AX. We detected focal colocalization of S100A11, Rad54B, and γH2AX in the nucleoplasm of HaCaT cells (Figure 3D). This result indicates that a significant subfraction of S100A11 and Rad54B is colocalized directly at sites of DNA damage. Many, but not all γH2AX foci colocalized with S100A11/Rad54B, clearly indicating that at any given time during the DSB repair process only a subpopulation of repair sites is associated with S100A11/Rad54B foci. Recently, an induction of p21 after transfer of S100A11 into the nucleus has been shown (Sakaguchi *et al.*, 2003). Therefore, we also assessed the dynamics of p21 protein expression in HaCaT cells treated with BLM (Figure 3E). Hereby, we were able to detect an increased expression of p21 already 30 min after BLM treatment by immunoblotting.

Additionally, we asked whether the S100A11/Rad54B complex is associated both, with other DNA repair processes such the nonhomologous end joining (NHEJ) or sites of DNA damage induced by stalled replication forks. To this end, we assessed the distribution of S100A11, Rad54B, and Ku80 in HaCaT cells treated with BLM. No or very little colocalization was detectable between S100A11, Rad54B, and Ku80 (Supplemental Figure S5). Interestingly, a colocalization between S100A11 and Rad54B was also detectable here. To assess if the S100A11/Rad54B complex is involved in repair processes triggered by arrested replication, we carried out three-color confocal immunostaining to simultaneously detect S100A11, Rad54B, and PCNA. This allowed investigation of HaCaT cells at different cell cycle phases. Because PCNA redistributes throughout S phase with the same dynamic pattern of endogenous replication factories, its localization pattern discriminates between early, mid- and late replication (Somanathan *et al.*, 2001). Neither in G1 or G2, nor at any stage of S phase did we observe a colocalization between S100A11/Rad54B and PCNA (Supplemental Figure S6). The S100A11/Rad54B complex was again detectable, above all in cells that are in G2 phase.

Figure 3 (cont). merged at different time points as indicated. (B) CoIP of Rad54B by a specific anti-S100A11 antibody from HaCaT cell extracts. HaCaT cells were treated with BLM for 3 h (lane 2) or 8 h (lane 3) or as a control, cells were untreated (lane 1). As a control for equal protein loading corresponding actin levels were shown by immunoblot. (C) Quantification of the increase in colocalization between S100A11 and Rad54B in HaCaT cells after DNA DSB induction. The colocalization coefficient was determined as described in *Materials and Methods* in nuclei of cells treated as described in A. At least 20 nuclei were analyzed per time point. Data are displayed as mean values (±SD). The colocalization coefficient was also determined from SC-35/S100A11 and SC-35/Rad54B colocalization experiments of cells after 3 h of BLM treatment. (D) Examples of fixed HaCaT cells that were analyzed by three-color immunostaining followed by laser scanning microscopy for S100A11 (green), Rad54B (blue), and γH2AX (red) at DNA damage sites 1 h after BLM treatment. The intensities of the immunofluorescences in one cell derived from the Rad54B signal (blue), the γH2AX signal (red) and the S100A11 signal (green) are shown in a linescan (left panel; bottom side of the overlay). In the other example cell (right panel), multiple colocalizations of S100A11/Rad54B complexes with γH2AX foci corresponding to DNA damage sites are labeled by arrows (yellow); Bar, 5 μm. (E) Increased expression of p21 was already detectable after 30 min (lane 2) in HaCaT cells treated by BLM. As a control for equal protein loading corresponding actin levels were shown below. Lane 1, control; lane 2, 0.5 h after BLM treatment; lane 3, 1 h after BLM treatment; lane 4, 3 h after BLM treatment; lane 5, 8 h after BLM treatment.

Appearance of Rad54B Foci Is Dependent on the S100A11 Protein Status

To assess whether S100A11 has an effect on Rad54B targeting to DNA damage sites, we used RNA interference to down-regulate S100A11 protein levels. A significant reduction of the S100A11 protein level was detectable 72 h after transfection. S100A11 down-regulated HaCaT cells that were treated for 1 h with BLM to induce DSBs demonstrated a diffuse nucleoplasmatic localization pattern of Rad54B that was clearly different from the foci-like pattern in untreated cells or cells treated with control siRNA (Figure 4A). In HaCaT cells transfected with control siRNA the colocalization between the S100A11/Rad54B foci at sites of DNA damage repair was indistinguishable from nontreated cells (compare Figures 4A and 3C). Most strikingly, colocalization between Rad54B and γH2AX was abolished in cells with down-regulated S100A11 levels. Thus, the appearance of Rad54B foci at DSB repair sites depends on the S100A11 protein status and not on the induction of DNA damages by BLM. Quantitation of the Rad54B nuclear localization pattern in S100A11 down-regulated versus control-treated cells confirmed the above observations (Figure 4B).

We finally assessed the impact of reduced S100A11 levels on p21 expression in HaCaT cells by Western blotting. Surprisingly, this analysis revealed a significant reduction in p21 protein levels when S100A11 expression was down-regulated by siRNA. This reduction of p21 was independent of BLM treatment of HaCaT cells (Figure 4C). The level of Rad54B persisted unaffected by down-regulation of S100A11. These observations demonstrate that S100A11 is required for both Rad54B accumulation at sites of DNA DSB repair and for maintenance of p21 levels during the DNA damage response.

Depletion of S100A11 Influenced the Proliferation Capacity of HaCaT Cells

To analyze a possible impairment of DNA repair by abolishing the S100A11–Rad54B interaction, we quantified the repair of DNA DSBs by immunofluorescence-based detection of γH2AX foci (Rogakou *et al.*, 1999; Kegel *et al.*, 2007). HaCaT cells were transfected with a specific S100A11 siRNA and γH2AX foci appearance was assessed after 1 or 3 h after BLM treatment. DSB repair by homologous recombination is nearly completed after 3 h (Chai *et al.*, 2005). Only minor or no differences in the number of γH2AX foci were detectable at the different time points in S100A11 down-regulated HaCaT cells compared with cells transfected with a control siRNA (Figure 5A). Because there is a correlation between γH2AX loss and DSB repair activity at low, but not high, cytotoxic doses (Bouquet *et al.*, 2006; Markova *et al.*, 2007), we analyzed the proliferation capacity of S100A11 down-regulated HaCaT cells compared with control cells. First, we assessed HaCaT cells transfected with control or S100A11-specific siRNA in colony-forming assays (Figure 5B). Thereby, we detected a significant decrease of colony formation of S100A11 down-regulated HaCaT cells compared with the control. This decrease of colony formation was even reinforced when HaCaT cells were treated with BLM for 30 min. When S100A11 was down-regulated in HaCaT cells, the proliferation capacity and thus the number of these cells was limited. Hence, we also investigated if the restricted proliferation capacity of S100A11 down-regulated cells is reflected in a change of cell cycle transition or increased apoptosis rate. Flow-cytometric analysis of S100A11 down-regulated HaCaT cells that were treated

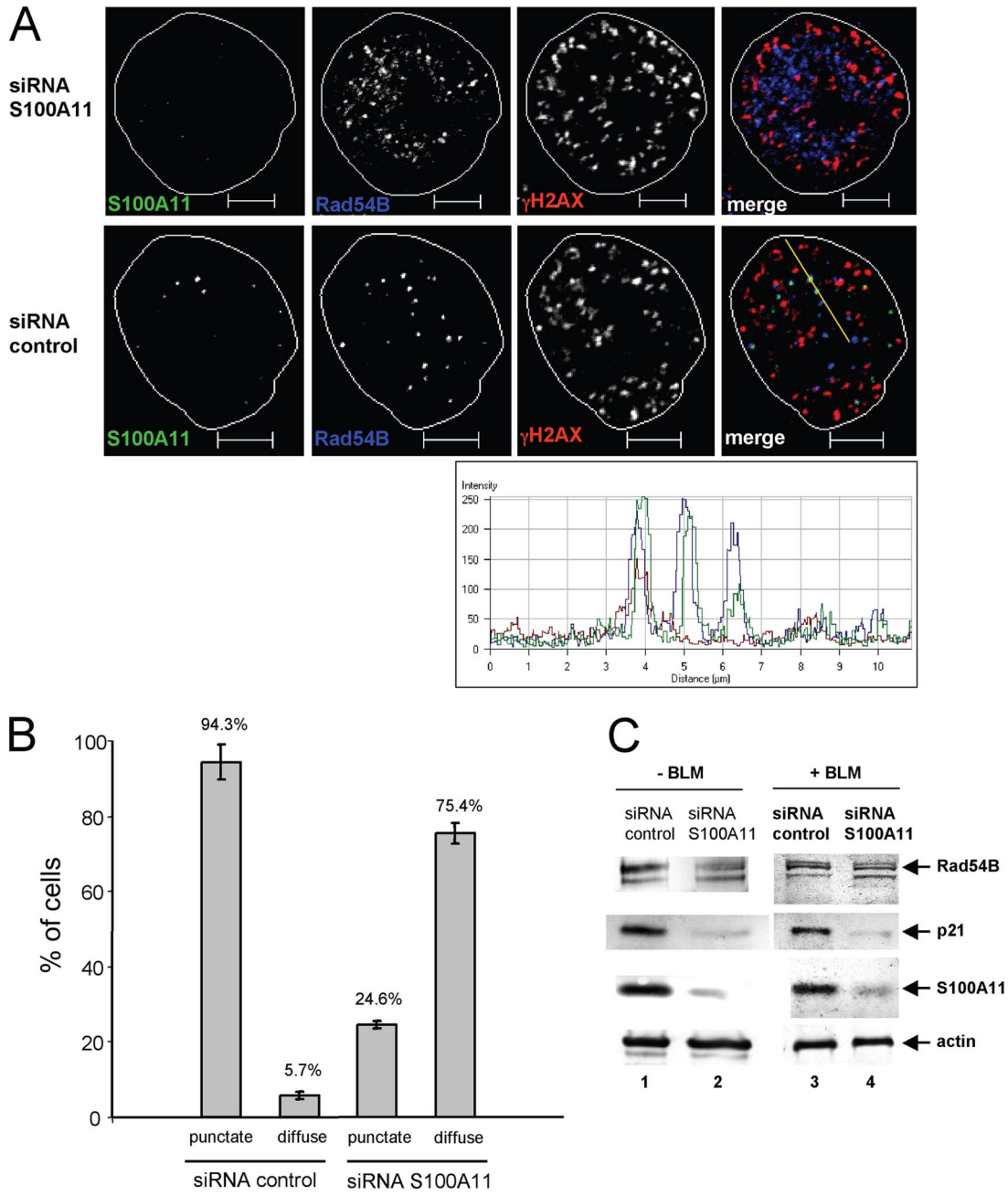

Figure 4. S100A11 is required for Rad54B foci formation. (A) HaCaT cells were transfected with specific siRNA for depletion of S100A11 (siRNA S100A11) or, as a control, nonsilencing siRNA (siRNA control), respectively, and treated by BLM for 1 h followed by immunostaining against S100A11 (green), Rad54B (blue), and γH2AX (red) using specific antibodies. The overlay image (merge) shows that S100A11/Rad54B foci formation significantly overlaps with sites of DNA damage repair in experiments using cells transfected with control siRNA (bottom panel). HaCaT cells transfected with specific S100A11 siRNA oligos show a diffuse nucleoplasmatic localization pattern of Rad54B and no colocalization with γH2AX (top panel). In the image derived from the control experiment, a merged signal with complete overlap between S100A11, Rad54B and γH2AX is indicated in a linescan (bottom panel). Bar, 5 μm. (B) Quantitation of alterations in the Rad54B nuclear distribution pattern after S100A11 knockdown. HaCaT cells were treated as in A and the nuclear distribution pattern of Rad54B was assessed in cells transfected with control siRNA (n = 70) or oligos specific for S100A11 (n = 65). (C) Down-regulation of p21 after knockdown of S100A11. Protein extracts of HaCaT cells transfected with specific S100A11 siRNA (lane 2) or, as a control, nonsilencing siRNA (lane 1), respectively, as well as HaCaT cells treated as in A (lanes 3 and 4) were subjected to immunoblotting against S100A11, p21, and Rad54B using specific antibodies. As a control for equal protein loading corresponding actin levels were shown by immunoblot.

with BLM revealed a significant increase of the sub-G1/apoptotic cell fraction compared with BLM treated control HaCaT cells (Figure 5C). The sub-G1/apoptotic cell fraction of control HaCaT cells was similar to those of wild-type HaCaT cells without BLM treatment. The simultaneous down-regulation of p21 in S100A11 down-regulated HaCaT cells might explain an accelerated transition in the cell cycle from G1 to S phase and thus a smaller G1 cell fraction compared with cells transfected with the control siRNA.

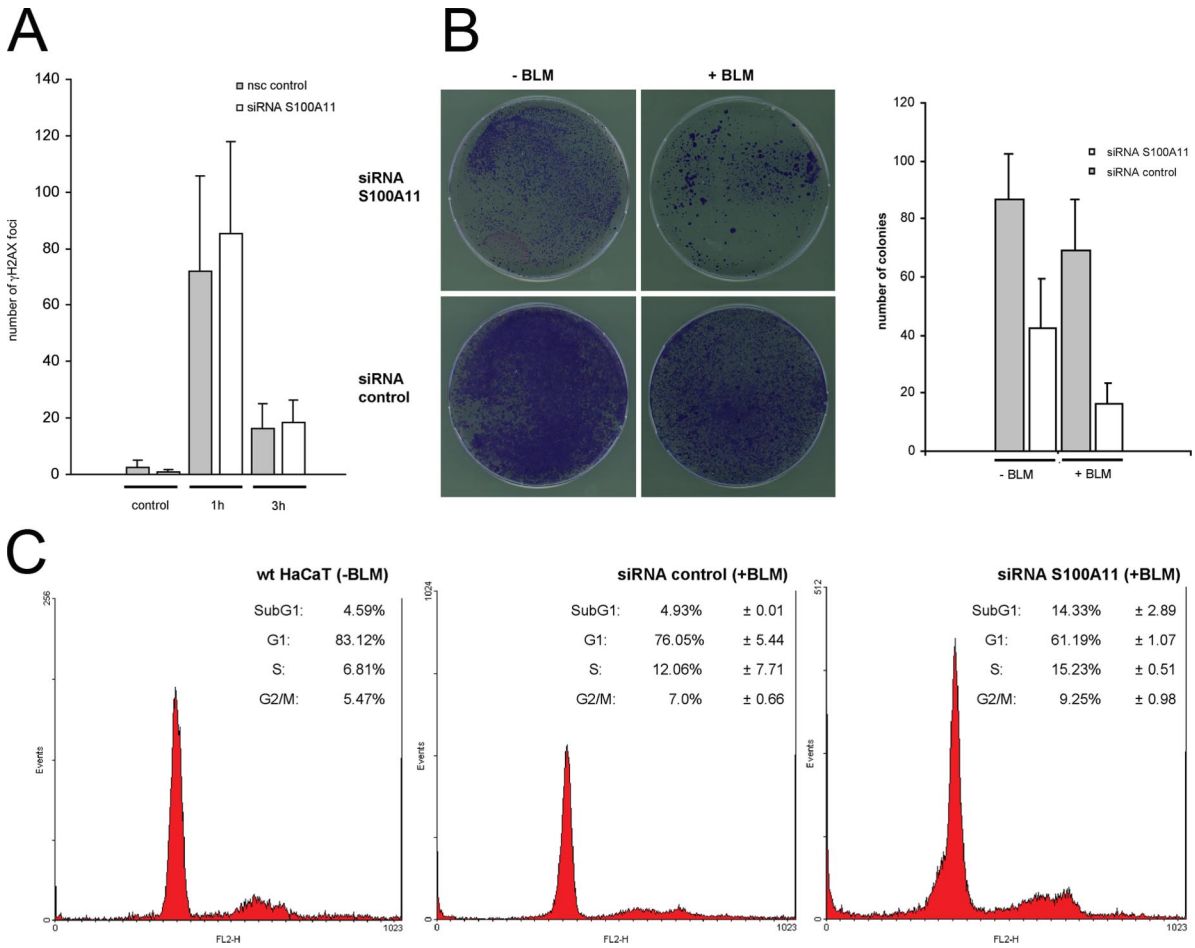

Figure 5. S100A11 down-regulated HaCaT cells possesses a restricted proliferation capacity. (A) Quantification of DNA DSB repair by immunofluorescence-based detection of γH2AX foci in HaCaT cells transfected with a specific S100A11 siRNA (white bars) or, as a control, with a nonsilencing control siRNA (gray bars). Transfected cells were treated with BLM for 30 min and number of γH2AX foci was counted 1 h and 3 h after BLM treatment as well as in untreated cells (control). (B) For analysis of the proliferation capacity of HaCaT cells colony forming assays were carried out. HaCaT cells were transfected as in A, treated by BLM 72 h after transfection and grown for a further 7 d (+BLM). As a control, transfected cells grown without BLM treatment (−BLM). For quantification, the colonies in 10 representative areas (0.5-cm diameter) of Petri dishes with transfected HaCaT cells with (+BLM) or without (−BLM) BLM treatment were counted. □, cells transfected with specific S100A11 siRNA; ▨, cells transfected with a nonsilencing control siRNA. (C) Flow-cytometric analysis of cell cycle phases of HaCaT cells transfected as in A, which were treated by BLM for 30 min. Additionally, the flow-cytometric analysis of wild-type HaCaT keratinocytes (HaCaT control [-BLM]) without BLM treatment is shown as a control. Percentage (±SD) of cells in cell cycle phases is displayed in the diagrams.

DISCUSSION

In this study we used a proteomic approach comprising SELDI mass spectrometry and immunological techniques to identify in vivo interacting partners of S100A11. In this way, we detected a protein complex between endogenously expressed S100A11 and Rad54B in the human keratinocyte cell line HaCaT. A possible functional connection between S100A11 and Rad54B was further characterized by immunofluorescence experiments followed by confocal microscopy. It is believed that this phosphorylation of S100A11 causes dissociation of S100A11 from actin filaments as a prerequisite for its nuclear translocation (Sakaguchi *et al.*, 2000). To simulate physiological conditions, we relinquished at additional Ca^{2+} in our protein–protein interaction detection approach. Previously, we showed that the detection of protein interactions of S100 proteins is not dependent on additional Ca^{2+} (Lehmann *et al.*, 2005). In addition, an increase of the Ca^{2+} concentration may result in an at least transient destabilization of protein complexes containing S100 proteins (Rosenberger *et al.*, 2007). The specific S100A11–Rad54B protein complex formation was further consistent with our two-color immunofluorescence experiments. Hereby, we detected extensive colocalization between S100A11 and Rad54B in small and discrete focal sites throughout the nucleoplasm of several cell lines. Rad54B plays an unique role in homologous recombination-mediated DNA damage repair and appears in complexes after replication arrest resulting from stalled replication forks (Otterlei *et al.*, 2006; Wesoly *et al.*, 2006). Collapsed replication forks can lead to DSBs that are repaired predominantly by homologous recombination (Amaudeau *et al.*, 2001). After induction of DNA damages one of the first cellular responses is phosphorylation of H2AX at the sites of DSB (Rogakou *et al.*, 1998). The subsequent time- and space-regulated accumulation of specific repair factors appears to be essential during DSB repair and signaling (Bekker-Jensen *et al.*, 2006). The accumulation of γH2AX foci has also been found in both apoptotic and senescent human cells

(Rogakou *et al.*, 2000; Sedelnikova *et al.*, 2004). Previously, it was described that γH2AX colocalizes with specific repair factors, for instance Rad51, at nuclear foci after DNA damage (Paull *et al.*, 2000). From our observations we conclude that both, Rad54B and S100A11 share this feature with other DNA repair factors. In this context we propose a novel function for S100A11 in the DNA double-strand process that likely involves DNA repair activity and/or signaling. Rad54B is able to stimulate homologous recombination by interaction with both Dmc1 and Rad51 (Sehorn *et al.*, 2004; Wesoly *et al.*, 2006). We show here that formation of the S100A11–Rad54B protein complex is stimulated by DNA damage and that the kinetics of complex formation appears to be directly correlated with the activity of the DSB repair machinery during successful repair cycles. Moreover, the focal colocalization pattern of S100A11/Rad54B was extensively, albeit not exclusively, spatially associated with sites of DSB repair as detected by γH2AX foci formation. The stimulation of the complex formation between S100A11 and Rad54B is obviously time dependent, with the highest number of S100A11–Rad54B complexes after approx. 3 h. These kinetics are also similar to the temporal stimulation of the Dmc1 recombinase-mediated DNA strand exchange activity by Rad54B (Sarai *et al.*, 2006). As reported, after transfer of S100A11 into the nucleus, an induction of the CDK inhibitor $p21^{WAF1/CIP1}$ is initiated (Sakaguchi *et al.*, 2003). In the present study, we were able to detect elevated p21 protein levels after treatment of HaCaT cells with BLM. The activation of p21 must be p53 independent because HaCaT cells possess only a mutated inactive form of p53 that is not able to induce p21 (Lehman *et al.*, 1993; Yoon and Smart, 2004). A Chk2-induced cellular senescence was associated with p21 expression that was also p53-independent (Chen *et al.*, 2005). The Chk2-induced senescence in HaCaT cells is dependent on a Chk2-mediated up-regulation of p21 (Aliouat-Denis *et al.*, 2005). A functional link between p21-mediated cell cycle regulation and Rad51 is suggested in mammalian cells because Rad51 expression, Rad51 foci formation, and p21 expression are interrelated. Furthermore, increase of p21 levels can be induced by Rad51 overexpression independent of p53 (Raderschall *et al.*, 2002).

As reported here, the S100A11–Rad54B complex occurred in discrete foci in the nucleoplasm of untreated cells as well as in cells treated by BLM where this complex was detectable directly at sites of DNA damages. This specific pattern changed completely when S100A11 was down-regulated by RNA interference. In this case, Rad54B appeared in a more diffuse nucleoplasmatic localization pattern and, most strikingly, Rad54B targeting to DSBs was abolished. An alteration of the Rad54B distribution pattern from a diffuse localization pattern to discrete foci representing stalled replication forks was also observed in HeLa cells treated with mitomycin (Otterlei *et al.*, 2006) at concentrations that induce DNA DSBs at such sites (Mogi and Oh, 2006). Our observations therefore indicate that S100A11 may be required to dynamically relocate Rad54B to or from sites of DSBs. We also demonstrated that elimination of Rad54B from sites of DSB repair after S100A11 depletion caused no significant differences in the number of γH2AX foci in compare to control cells. These data correlate with a report that demonstrated very little sensitivity of Rad54B knockout HCT116 cells to ionizing radiation (IR) and mitomycin C (MMC) compared with wild-type cells (Miyagawa *et al.*, 2002). When Rad54B targeting to DSB is abolished, the homolog protein Rad54 might adopt this task in the repair processes. It was recently shown that Rad54B-deficient mice ES cells possess only slight sensitivity to IR and MMC and a more pronounced phenotype in response to MMC in the additional absence of Rad54 (Wesoly *et al.*, 2006). Interestingly, p21 protein levels were also reduced in repairing cells when S100A11 was down-regulated. This observation suggests that S100A11, besides its Rad54B targeting function, is also involved in the regulation of p21 protein levels. In this context, we report here that S100A11 down-regulation caused a restriction of the proliferation capacity of HaCaT keratinocytes. Concurrently, an increase of the apoptotic cell fraction of S100A11 down-regulated HaCaT cells was detectable. This is not surprising as p21 can act, beside its function in the DNA damage response, as an inhibitor of apoptosis in a number of systems (Gartel and Tyner, 2002). On the basis of these observations we speculate that S100A11 provides a direct link between the repair machinery at DNA DSBs and the signaling machinery that controls cell cycle progression. We currently investigate this possible connection.

ACKNOWLEDGMENTS

We thank Dr. Patrick Sung (Yale University School of Medicine) for critical advice and Ralf Schmidt for technical assistance. This study was supported by a grant from the Wilhelm Sander-Stiftung to C.M.

REFERENCES

Aliouat-Denis, C. M. *et al.* (2005). p53-independent regulation of p21Waf1/Cip1 expression and senescence by Chk2. Mol. Cancer Res. *3*, 627–634.

Amaudeau, C., Lundin, C., and Helleday, T. (2001). DNA double-strand breaks associated with replication forks are predominantly repaired by homologous recombination involving an exchange mechanism in mammalian cells. J. Mol. Biol. *307*, 1235–1245.

Bekker-Jensen, S., Lukas, C., Kitagawa, R., Melander, F., Kastan, M. B., Bartek, J., and Lukas, J. (2006). Spatial organization of the mammalian genome surveillance machinery in response to DNA strand breaks. J. Cell Biol. *173*, 195–206.

Bisotto, S., Lauriault, P., Duval, M., and Vincent, M. (1995). Colocalization of a high molecular mass phosphoprotein of the nuclear matrix (p255) with spliceosomes. J. Cell Sci. *108*, 1873–1882.

Boni, R., Burg, G., Dogouglu, A., Ilg, E. C., Schafer, B. W., Muller, B., and Heizmann, C. W. (1997). Immunohistochemical localization of the Ca^{2+} binding S100 proteins in normal human skin and melanocytic lesions. Br. J. Dermatol. *137*, 39–43.

Boukamp, P., Petrussevska, R. T., Breitkreutz, D., Hornung, J., Markham, A., and Fusenig, N. E. (1988). Normal keratinization in a spontaneously immortalized aneuploid human keratinocyte cell line. J. Cell Biol. *106*, 761–771.

Bouquet, F., Muller, C., and Salles, B. (2006). The loss of gammaH2AX signal is a marker of DNA double strand breaks repair only at low levels of DNA damage. Cell Cycle *5*, 1116–1122.

Broome, A. M., Ryan, D., and Eckert, R. L. (2003). S100 protein subcellular localization during epidermal differentiation and psoriasis. J. Histochem. Cytochem. *51*, 675–685.

Chai, B., Huang, J., Cairns, B. R., and Laurent, B. C. (2005). Distinct roles for the RSC and Swi/Snf ATP-dependent chromatin remodelers in DNA double-strand break repair. Genes Dev. *19*, 1656–1661.

Chaurand, P., DaGue, B. B., Pearsall, R. S., Threadgill, D. W., and Caprioli, R. M. (2001). Strain-based sequence variations and structure analysis of murine prostate specific spermine binding protein using mass spectrometry. Proteomics *1*, 1320–1326.

Chen, C. R., Wang, W., Rogoff, H. A., Li, X., Mang, W., and Li, C. J. (2005). Dual induction of apoptosis and senescence in cancer cells by Chk2 activation: checkpoint activation as a strategy against cancer. Cancer Res. *65*, 6017–6021.

Donato, R. (2001). S100, a multigenic family of calcium-modulated proteins of the EF-hand type with intracellular and extracellular functional roles. Int. J. Biochem. Cell Biol. *33*, 637–668.

Dulic, V., Kaufmann, W. K., Wilson, S. J., Tlsty, T. D., Lees, E., Harper, J. W., Elledge, S. J., and Reed, S. I. (1994). p53-dependent inhibition of cyclin-dependent kinase activities in human fibroblasts during radiation-induced G1 arrest. Cell *76*, 1013–1023.

Eckert, R. L., Broome, A. M., Ruse, M., Robinson, N., Ryan, D., and Lee, K. (2004). S100 proteins in the epidermis. J. Invest. Dermatol. *123*, 23–33.

El-Deiry, W. S., Tokino, T., Velculescu, V. E., Levy, D. P., Parson, R., Trent, J. M., Lin, D., Mercer, W. E., Kinzler, K. W., and Vogelstein, B. (1993). WAF1, a potential mediator of p53. Cell *75*, 817–825.

Escher, N., Kob, R., Tenbaum, S. P., Eisold, M., Baniahmad, A., von Eggeling, F., and Melle, C. (2007). Various members of the E2F transcription factor family interact in vivo with the corepressor Alien. J. Proteome Res. *6*, 1158–1164.

Fang, Z., Fu, Y., Liang, Y., Li, Z., Zhang, W., Jin, J., Yang, Y., and Zha, X. (2007). Increased expression of integrin beta1 subunit enhances p21(WAF1/Cip1) transcription through the Sp1 sites and p300-mediated histone acetylation in human hepatocellular carcinoma cells. J. Cell. Biochem. *101*, 654–664.

Gartel, A. L., and Tyner, A. L. (1999). Transcriptional regulation of the p21(WAF1/CIP1) gene. Exp. Cell Res. *246*, 280–289.

Gartel, A. L., and Tyner, A. L. (2002). The role of the cyclin-dependent kinase inhibitor p21 in apoptosis. Mol. Cancer Ther. *1*, 639–649.

Hoeijmakers, J. H. (2001). Genome maintenance mechanisms for preventing cancer. Nature *411*, 366–374.

Inada, H., Naka, M., Tanaka, T., Davey, G. E., and Heizmann, C. W. (1999). Human S100A11 exhibits differential steady-state RNA levels in various tissues and a distinct subcellular localization. Biochem. Biophys. Res. Commun. *263*, 135–138.

Kegel, P., Riballo, E., Kühne, M., Jeggo, P. A., and Löbrich, M. (2007). X-irradiation of cells on glass slides has a dose doubling impact. DNA Repair *6*, 1692–1697.

Kob, R., Baniahmad, A., Escher, N., von Eggeling, F., and Melle, C. (2007). Detection and identification of transcription factors as interaction partners of Alien in vivo. Cell Cycle *6*, 393–396.

Lehman, T. A. *et al.* (1993). p53 mutations in human immortalized epithelial cell lines. Carcinogenesis *14*, 833–839.

Lehmann, R., Melle, C., Escher, N., and von Eggeling, F. (2005). Detection and identification of protein interactions of S100 proteins by ProteinChip technology. J. Proteome Res. *4*, 1717–1721.

Lettier, G., Feng, Q., de Mayolo, A. A., Erdinez, N., Reid, R. J., Lisby, M., Mortensen, U. H., and Rothstein, R. (2006). The role of DNA double-strand breaks in spontaneous homologous recombination in *S. cerevisiae.* PLoS Genet. *2*, e194.

Manders, E.M.M., Verbeek, F. J., and Aten, J. A. (1993). Measurement of co-localization of objects in dual color confocal images. J. Microscopy *169*, 375–382.

Markova, E., Schultz, N., and Belyaev, I. Y. (2007). Kinetics and dose-response of residual 53BP1/gamma-H2AX foci: xo-localization, relationship with DSB repair and clonogenic survival. Int. J. Radiat. Biol. *83*, 319–329.

Melle, C., Ernst, G., Schimmel, B., Bleul, A., Mothes, H., Settmacher, U., and von Eggeling, F. (2006). Different expression of calgizzarin (S100A11) in normal colonic epithelium, adenoma and colorectal carcinoma. Int. J. Oncol. *28*, 195–200.

Miyagawa, K., Tsuruga, T., Kinomura, A., Usui, K., Katsura, M., Tashiro, S., Mishima, H., and Tanaka, K. (2002). A role for RAD54B in homologous recombination in human cells. EMBO J. *21*, 175–180.

Mogi, S., and Oh, D. H. (2006). gamma-H2AX formation in response to interstrand crosslinks requires XPF in human cells. DNA Repair *5*, 731–740.

Otterlei, M., Bruheim, P., Ahn, B., Bussen, W., Karmakar, P., Bayton, K., and Bohr, V. A. (2006). Werner syndrome protein participates in a complex with RAD51, RAD54, RAD54B and ATR in response to ICL-induced replication arrest. J. Cell Sci. *119*, 5137–5146.

Paull, T. T., Rogakou, E. P., Yamazaki, V., Kirchgessner, C. U., Gellert, M., and Bonner, W. M. (2000). A critical role for histone H2AX in recruitment of repair factors to nuclear foci after DNA damage. Curr. Biol. *10*, 886–895.

Raderschall, E. *et al.* (2002). Formation of higher-order nuclear Rad51 structures is functionally linked to p21 expression and protection from DNA damage-induced apoptosis. J. Cell Sci. *115*, 153–164.

Rogakou, E. P., Pilch, D. R., Orr, O. H., Ivanova, V. S., and Bonner, W. M. (1998). DNA double-stranded breaks induce histone H2AX phosphorylation on serine 139. J. Biol. Chem. *273*, 5858–5868.

Rogakou, E. P., Boon, C., Redon, C., and Bonner, W. M. (1999). Megabase chromatin domains involved in DNA double-strand breaks in vivo. J. Cell Biol. *146*, 905–916.

Rogakou, E. P., Nieves-Neira, W., Boon, C., Pommier, Y., and Bonner, W. M. (2000). Initiation of DNA fragmentation during apoptosis induces phosphorylation of H2AX histone at serine 139. J. Biol. Chem. *275*, 9390–9395.

Rosenberger, S., Thorey, I. S., Werner, S., and Boukamp, P. (2007). A novel regulator of telomerase. S100A8 mediates differentiation-dependent and calcium-induced inhibition of telomerase activity in the human epidermal keratinocyte line HaCaT. J. Biol. Chem. *282*, 6126–6135.

Sakaguchi, M., Miyazaki, M., Inoue, Y., Tsuji, T., Kouchi, H., Tanaka, T., Yamada, H., and Namba, M. (2000). Relationship between contact inhibition and intranuclear S100C of normal human fibroblasts. J. Cell Biol. *149*, 1193–1206.

Sakaguchi, M., Miyazaki, M., Takaishi, M., Sakaguchi, Y., Makino, E., Kataoka, N., Yamada, H., Namba, M., and Huh, N. H. (2003). S100C/A11 is a key mediator of Ca^{2+}-induced growth inhibition of human epidermal keratinocytes. J. Cell Biol. *163*, 825–835.

Sakaguchi, M., Miyazaki, M., Sonegawa, H., Kashiwagi, M., Ohba, M., Kuroki, T., Namba, M., and Huh, N. H. (2004). PKCα mediates TGFβ-induced growth inhibition of human keratinocytes via phosphorylation of S100C/A11. J. Cell Biol. *164*, 979–984.

Sakaguchi, M., Sonegawa, H., Murata, H., Kitazoe, M., Futami, J. I., Kataoka, K., Yamada, H., and Huh, N. H. (2008). S100A11, a dual mediator for growth regulation of human keratinocytes. Mol. Biol. Cell *19*, 78–85.

Sarai, N., Kugawa, W., Kinebuchi, T., Kagawa, A., Tanaka, K., Miyagawa, K., Ikawa, S., Shibata, T., Kurumizaka, H., and Yokoyama, S. (2006). Stimulation of Dmc1-mediated DNA strand exchange by the human Rad54B protein. Nucleic Acids Res. *34*, 4429–4437.

Schafer, B. W., and Heizmann, C. W. (1996). The S100 family of EF-hand calcium-binding proteins: functions and pathology. Trends Biochem. Sci. *21*, 134–140.

Sedelnikova, O. A., Horikawa, I., Zimonjic, D. B., Popescu, N. C., Bonner, W. M., and Barrett, J. C. (2004). Senescing human cells and ageing mice accumulate DNA lesions with unrepairable double-strand breaks. Nat. Cell Biol. *6*, 168–170.

Sehorn, M. G., Sigurdsson, S., Bussen, W., Unger, V. M., and Sung, P. (2004). Human meiotic recombinase DMC1 promotes ATP-dependent homologous DNA strand exchange. Nature *429*, 433–437.

Somanathan, S., Suchyna, T. M., Siegel, A. J., Berezney, R. (2001). Targeting of PCNA to sites of DNA replication in the mammalian cell nucleus. J. Cell. Biochem. *81*, 56–67.

Tanaka, K., Kagawa, W., Kinebuchi, T., Kurumizaka, H., H., and Miyagawa, K. (2002). Human Rad54B is a double-stranded DNA-dependent ATPase and has biochemical properties different from its structural homolog in yeast, Tid1/Rdh54. Nucleic Acids Res. *30*, 1346–1353.

Tsuda, M., Watanabe, T., Seki, T., Kimura, T., Sawa, H., Minami, A., Akagi, T., Isobe, K., Nagashima, K., and Tanaka, S. (2005). Induction of p21(WAF1/CIP1) by human synovial sarcoma-associated chimeric oncoprotein SYT-SSX1. Oncogene *24*, 7984–7990.

van Ginkel, R. P., Gee, R. L., Walker, T. M., Hu, D. N., Weizmann, C. W., and Polans, A. S. (1998). The identification and differential expression of calcium-binding proteins associated with ocular melanoma. Biochim. Biophys. Acta *1448*, 290–297.

von Mikecz, A., Zhang, S., Montminy, M., Tan, E. M., and Hemmerich, P. (2000). CREB-binding protein (CBP)/p300 and RNA polymerase II colocalize in transcriptionally active domains in the nucleus. J. Cell Biol. *150*, 265–273.

Wesoly, J. *et al.* (2006). Different contributions of mammalian Rad54 paralogs to recombination, DNA damage repair, and meiosis. Mol. Cell. Biol. *26*, 976–989.

Wolner, B., van Komen, S., Sung, P., and Peterson, C. L. (2003). Recruitment of the recombinational repair machinery to a DNA double-strand break in yeast. Mol. Cell *12*, 221–232.

Yoon, K., and Smart, R. C. (2004). C/EBPα is a DNA damage-inducible p53-regulated mediator of the G_1 checkpoint in keratinocytes. Mol. Cell. Biol. *24*, 10650–10660.

Xhao, X. O., Naka, M., Muneyuki, M., and Tanaka, T. (2000). Ca(2+)-dependent inhibition of actin-activated myosin ATPase activity by S100C (S100A11), a novel member of the S100 protein family. Biochem. Biophys. Res. Commun. *267*, 77–79.